Journal of Alloys and Compounds 555 (2013) 315–319

Contents lists available at SciVerse ScienceDirect

Journal of Alloys and Compounds

journal homepage: www.elsevier.com/locate/jalcom

Evidence of defect-mediated magnetic coupling on hydrogenated Co-doped ZnO

M.P.F. de Godoy [a], A. Mesquita [b], W. Avansi [c], P.P. Neves [b], V.A. Chitta [d], W.B. Ferraz [e], M.A. Boselli [f], A.C.S. Sabioni [g], H.B. de Carvalho [b,*]

[a] Departamento de Física, Universidade Federal de São Carlos, 13565-905 São Carlos-SP, Brazil
[b] Universidade Federal de Alfenas, 37130-000 Alfenas-MG, Brazil
[c] INCTMN, LIEC, Instituto de Química, UNESP, 14800-900 Araraquara-SP, Brazil
[d] Instituto de Física, Universidade de São Paulo, P.O. Box 66318, 05315-970 São Paulo-SP, Brazil
[e] Centro de Desenvolvimento de Tecnologia Nuclear/CNEN, 31270-901 Belo Horizonte-MG, Brazil
[f] Universidade Federal de Uberlândia, 38400-902 Uberlândia-MG, Brazil
[g] Universidade Federal de Ouro Preto, 35400-000 Ouro Preto-MG, Brazil

ARTICLE INFO

Article history:
Received 25 August 2012
Received in revised form 5 November 2012
Accepted 10 November 2012
Available online 29 November 2012

Keywords:
Solid state reactions
Oxide materials
Magnetically ordered materials
X-ray diffraction
Scanning tunnelling microscopy
STM, Synchrotron radiation
Magnetic measurements

ABSTRACT

Hydrogenated bulk $Zn_{1-x}Co_xO$ samples were synthesized via standard solid-state reaction route with Co molar concentrations up to 15 at.%. Magnetic characterization demonstrates a room temperature ferromagnetic behavior associated to a paramagnetic Curie–Weiss component. Detailed microstructural analysis was carried out to exclude the presence of extrinsic sources of ferromagnetism. The magnetization increases linearly as a function of Co concentration. Hall measurements reveal an insulating character for the whole set of samples. In this context, the defect mediated magnetic coupling between the Co atoms under the scope of the bound magnetic polarons model is used to interpret the observed room temperature ferromagnetism.

1. Introduction

The theoretical prediction of room temperature ferromagnetism (RTFM) in transition metal (TM) doped large band gap semiconductors [1] promoted the research on such kind of systems as one of the most active and attractive topic in materials science and condensed-matter physics. The manipulation of both charge and spin of carriers in semiconductors turns the development of spintronic devices with all its new functionalities attainable. In this direction, a huge effort has been concentrated on TM-doped oxide semiconductors as ZnO, TiO_2 and SnO_2 [2–4]. In spite of the extensive investigations, the origin of the observed RTFM remains inconclusive and controversial. Early works on such systems attributed the observed RTFM to a carrier-mediated mechanism [5]. However, there is a growing consensus that defects play an important role to drive the ferromagnetic behavior. In this scenario, the main theoretical models proposed to describe the origin and properties of ferromagnetism suppose that electrons introduced by donor defects into the conduction band [6] or forming bound magnetic polarons (BMP) [7] mediate ferromagnetic couplings between TM ions. Another important model, attempting to explain the observed RTFM in undoped systems [8], assigns the ferromagnetic response to spins of electrons residing on point or extended defects, the called d^0 ferromagnetism [9].

In the present work we report a study of the structural and the magnetic properties of hydrogenated $Zn_{1-x}Co_xO$ bulk samples with Co molar concentrations up to 15 at.%. Our previous work showed that the presence of substitutional Co on ZnO matrix was not a sufficient condition to achieve RTFM [10]. Besides, recent reports presented direct evidences of the correlation between the concentration of oxygen vacancies (V_O) and the observed RTFM [11–14]. As pointed by Kohan et al., oxygen/zinc vacancy is the main defect in the ZnO matrix under zinc/oxygen-rich conditions [15]. Therefore, V_O can be introduced into the system by annealing the samples in oxygen-poor atmospheres. This effect can be enhanced using a reduction gas to perform the annealing; in the case of using hydrogen gas, the annealing process is called hydrogenation [16]. The hydrogenation of our paramagnetic set of samples [10] added a ferromagnetic phase, confirming reports of robust enhancement of magnetization at room temperature, especially for Co-doped ZnO systems, under this annealing process [17,18]. The hydrogenation is intended to be responsible to introduce a

* Corresponding author. Tel.: +55 35 8837 0132; fax: +55 35 3299 1384.
E-mail addresses: bonette@unifal-mg.edu.br, bonette@gmail.com (H.B. de Carvalho).

0925-8388/$ - see front matter © 2012 Elsevier B.V. All rights reserved.
http://dx.doi.org/10.1016/j.jallcom.2012.11.105

properly density of defects in the structure of the samples that couples ferromagnetically the magnetic moments of the dopants.

2. Experiment

Polycrystalline $Zn_{1-x}Co_xO$ (x = 0.08, 0.12 and 0.15) bulk samples were prepared by standard solid state reaction method following procedures described in Ref. [10]. These samples were here labeled as-prepared samples and only present a paramagnetic behavior. The as-prepared samples were then annealed in an atmosphere of Ar (95%) and H_2 (5%) for 3 h at 600 °C. The effects of hydrogenation on the structural properties were investigated by X-ray diffraction (XRD) recorded in the range of 2θ = 30–70° with steps of 0.01° at 3 s/step. Structural analysis was performed using the Rietveld method as implemented by the software General Structure Analysis System (GSAS) package with the graphical user interface EXPGUI [19,20]. The microstructure and the composition distribution were characterized by scanning electron microscopy (SEM), high-resolution transmission electron microscopy (HRTEM) and an energy dispersive X-ray spectrometry (EDS). Co K-edge X-ray absorption near-edge structure (XANES) and extended X-ray absorption fine structure (EXAFS) was used to determine the valence state and to evaluate the environment of Co in the ZnO lattice. The measurements were performed in the transmittance mode at the XAS beamline from the Brazilian Synchrotron Light Laboratory (LNLS), Campinas, Brazil. Magnetic measurements were performed using a superconducting quantum interference device magnetometer (SQUID).

3. Results and discussion

Fig. 1(a) shows the X-ray diffraction (XRD) results for the whole set of samples with the refined Rietveld pattern. The observed peaks correspond to those expected for polycrystalline wurtzite ZnO. Furthermore, the line-widths of the diffraction peaks are relatively quite narrow, revealing the good crystallinity quality of the samples. No additional phases were observed within the XRD detection limit (Fig. 1(b)). The Rietveld refinement initiated with

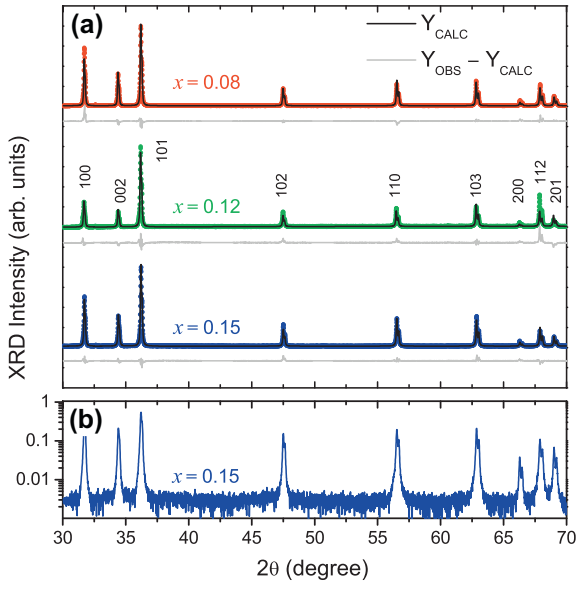

Fig. 1. (a) Refined XRD diffractograms of polycrystalline $Zn_{1-x}Co_xO$ bulk samples. Each figure shows the observed pattern (symbols), Rietveld calculated pattern (solid line), and the goodness of the fit or residual pattern (at the bottom). (b) Same diffraction pattern obtained for sample x = 0.15 presented in (a), but in a logarithm scale to highlight the absence of diffraction peaks associated to secondary phases.

Zn^{+2} and O^{-2} atoms located at (1/3, 2/3, 0) and (1/3, 2/3, z), respectively. The fitted curves match quite well with the experimental data. Table 1 presents the determined cell parameters along the atomic positional parameters, all this data are quite similar to those reported for pure ZnO [21]. Tetrahedrally coordinated Co^{+2} has an ionic radii of 0.58 Å and would not introduce high order unit cell distortions when substituting the tetrahedrally coordinated Zn^{2+} that has a close ionic radii of 0.60 Å [22]. These results indicate the Zn substitution by Co in the ZnO host matrix. Another important result of Rietveld refinement is the oxygen occupation factor (O_{occup}), which can give us an estimative of the concentration of the V_O. Taking into account the error in the determination of this parameter, we can say that the obtained V_O content is almost constant, 1.7% (0.017), for the whole set of samples. This result is reasonable, since all the samples were synthesized and annealed in the same conditions.

In order to probe the possible presence of secondary phases or chemical phase separation, high-resolution transmission electron microscopy (HRTEM) studies were performed on cross-sectional samples prepared by standard mechanical polishing followed by Ar^+-ion milling at 4.5 kV under 8° angle (Gatan PIPS system) for about 30 min. HRTEM characterization was performed on a JEOL JEM 2100 URP, operated at 200 keV. Fig. 2(a) presents an example of HRTEM images acquired for the sample with higher Co content (x = 0.15). We can see that the distance between neighboring planes is about 0.25 nm, related to the (101) crystallographic plane of wurtzite ZnO, as observed in XRD (Fig. 1). To improve the statistical analysis of the HRTEM studies we have also taken a series of scanning electron microscope (SEM) images over large areas of the polish surface of the sample (x = 0.15). The images were acquired using a backscattered electron detector (BSE) of a SEM-LV JEOL JSM 5900 that has a resolution down to 3 nm at 30 kV (Fig. 2(b)). The effective Co concentrations of the $Zn_{1-x}Co_xO$ samples (x_E) were also measured by energy dispersive X-ray spectrometer (EDS) and are presented in Fig. 2(c) as a function of the nominal Co concentration (x_N). The values x_E are explicitly presented in Table 3. We observe a good agreement between the measured and the nominal concentration values. It is worth to point that electron microscopy results do not reveal any evidence of crystallographic secondary phase or local aggregation of Co ions (Co-rich nanoclusters), strongly suggesting that the studied samples are in diluted state in the Co concentration range up to 15%, in good agreement with XRD results.

XANES spectra at room temperature showed in Fig. 3(a) give information on the coordination symmetry and the valence of ions incorporated in a solid. All samples exhibit similar K-edge white line shapes to those previously reported for tetrahedrally coordinated TM-doped ZnO [23]. The valence of the dopant ions can be analyzed by comparing their resulting edge structure to those obtained from reference samples (metallic Co, CoO and Co_2O_3). The XANES results undoubtedly indicate that Co on our samples assumes predominantly the 2+ oxidation state, which corroborates the XRD, HRTEM and SEM results.

Fig. 3(b) and (c) shows the extended X-ray absorption fine structure (EXAFS) oscillations and their correspondent Fourier transforms (FT), respectively. The EXAFS data were obtained at Co K-edge for the $Zn_{1-x}Co_xO$ samples, a Co foil and Co oxides pow-

Table 1
Structural data for $Zn_{1-x}Co_xO$ samples obtained through the Rietveld refinement. O_{occup} is the oxygen occupation factor, χ^2 is the square of goodness-of-fit indicator, and R_{WP} is the refinement quality parameter.

Sample (x)	a (Å)	c/a	V (Å^3)	z (O)	O_{occup}	χ^2	R_{WP}
0.08	3.25164(1)	1.6009	47.665(2)	0.3825(2)	0.984(4)	3.31	3.80
0.12	3.25385(1)	1.5993	47.714(1)	0.3823(2)	0.980(5)	3.52	2.41
0.15	3.25269(1)	1.5998	47.680(1)	0.3825(4)	0.985(4)	2.91	2.90

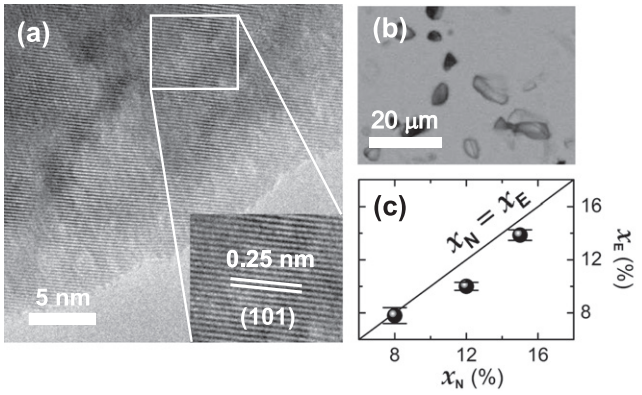

Fig. 2. Representative electron micrographs of $Zn_{1-x}Co_xO$ sample with $x = 0.15$. (a) Cross-sectional HRTEM image. (b) Scanning electron micrographs (Mag: 900×). (c) Effective Co concentrations obtained from EDS (x_E) versus nominal concentration (x_N).

ders. The results obtained at Zn *K*-edge for a pure ZnO reference sample prepared under the same conditions of doped samples are also presented. We observe that the EXAFS data for Co-doped samples are very similar to each other but quite different to those for the Co foil and the Co oxides. On the other hand, we observe that the EXAFS data are quite comparable to those obtained at Zn *K*-edge for the pure ZnO. This result is clear evidence that the Co is seated at the same environment of Zn atoms in the ZnO host matrix.

The extraction and fitting of EXAFS spectra were performed using Multi-Platform Applications for X-ray absorption (MAX) [24]. *Ab initio* FEFF8.2 code was used to calculate the theoretical spectra [25]. To obtain quantitative structural data concerning the first coordination shells, the neighborhood of Co atoms was modeled through the two main peaks (between 1.0 and 3.5 Å) from FT-EXAFS in Fig. 3(c). In all fits, we considered single and multi-scattering paths corresponding to the four successive atomic shells around Co substitutionally placed at Zn-sites of the ZnO host matrix according to the hexagonal wurtzite with $P6_3mc$ space group. Fig. 3(c) shows a good agreement between experimental (symbols) and simulated (lines) results for $Zn_{1-x}Co_xO$ samples. Table 2 lists the best fits to the data. The first shell (Co–O) coordination number is 4, consistent with a substitution for tetrahedral Zn^{2+} ions in the ZnO structure; besides the shell Co–Zn coordination number decreases as Co concentration increases as we would expect.

The structural analysis confirms that Co ions are diluted occupying Zn-sites of the ZnO wurtzite structure in hydrogenated $Zn_{1-x}Co_xO$. Clearly, the result excludes the presence of magnetic extrinsic sources as Co-rich nanocrystals and segregated secondary magnetic phases. With these conclusions we proceed to the magnetic characterization. The magnetic measurements were performed in a cryogenics superconducting quantum interference device (SQUID) system under magnetic fields up to 60 kOe in the range of 50–300 K. The results show the coexistence of two phases: a paramagnetic phase, similar to that observed in the as-prepared samples [10], and a ferromagnetic phase introduced by the hydrogenation. The coexistence of this two phases can be explained in terms of the efficiency of the hydrogenation process. The thermal annealing process is not able to reach the whole volume of our bulk sample, leaving most part of the material as before, keeping its paramagnetic behavior. To quantify the magnetic parameters of the coexisting two phases, we used the following function for the magnetic moment M as a function of magnetic field H [26]:

$$M(H) = \frac{2M_S}{\pi}\tan^{-1}\left[\frac{H \pm H_C}{H_C}\tan\left(\frac{\pi M_R}{2M_S}\right)\right] + \chi_P H. \quad (1)$$

Here the first term corresponds to a ferromagnetic hysteresis curve with the saturation magnetization M_S, the remanence M_R and the coercive field H_C. The second term is related to the corresponding paramagnetic susceptibility χ_P. Fig. 4 shows the ferromagnetic phase at 300 K obtained after the subtraction of paramagnetic phase. The fitting parameters M_S and χ_P are presented in Table 3. At room temperature H_C stays between 200 and 300 Oe (lower-right inset of Fig. 4). The coercivity H_C, likewise the remanence M_R, slightly decreases as function of temperature (not shown). We observe a linear increasing of M_S as a function of Co concentration (upper-left inset of Fig. 4).

The magnetic moment per Co atom (μ) in our hydrogenated samples can be derived from the following calculation. Since we have a coexistence of paramagnetic and a ferromagnetic phase, the total magnetization of the system is expressed as $M_T = M_P + M_{FM}$, where $M_P = \chi_P H$. At high temperatures the paramagnetic susceptibility can be written as $\chi_P = N_P\mu^2/3k_BT$, where N_P is the number of Co atoms in the paramagnetic phase

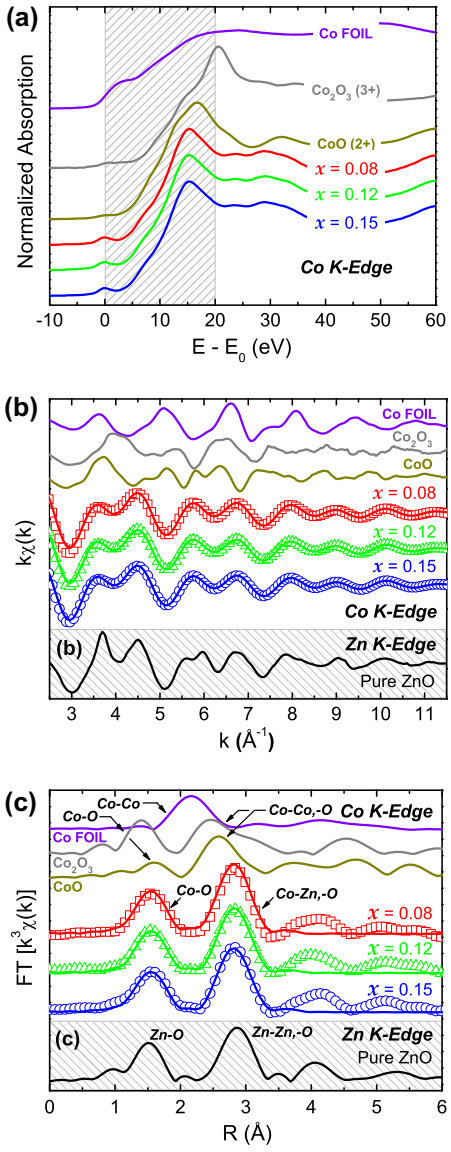

Fig. 3. (a) Experimental Co *K*-edge XANES spectra for the three $Zn_{1-x}Co_xO$ samples ($E_0 = 7708.8$ eV). Spectra of metallic Co, rocksalt CoO (valence 2+) and Co_2O_3(valence 3+) are also shown for comparison. (b) EXAFS oscillations with fits and (c) corresponding k^3 weighted Fourier transforms of Co and Zn *K*-edge data of bulk samples and reference powders. The spectra are offset for clarity.

Table 2
Co *K*-edge EXAFS simulation results obtained by assuming Co substitutionally placed at ZnO metal sites. *R*, with uncertainty 0.02 Å, is the distance from the central atom, *N* is the average coordination number, σ^2 the Debye–Waller factor, with uncertainty 0.0017 Å^2, and *Q* the quality factor [27].

Sample (x)	Shell	R(Å)	N	σ^2($\times10^{-3}$ Å^2)	Q
0.08	Co–O	1.98	4.5 ± 0.5	5.1	2.36
	Co–Zn	3.22	8.9 ± 0.7	5.2	
	Co–Zn	3.34	5.7 ± 2.9	5.2	
	Co–O	3.80	8.3 ± 1.4	5.1	
0.12	Co–O	1.98	4.1 ± 0.5	4.5	1.05
	Co–Zn	3.20	5.7 ± 0.4	2.7	
	Co–Zn	3.35	4.4 ± 0.4	2.7	
	Co–O	3.82	9.0 ± 0.2	4.5	
0.15	Co–O	1.98	4.2 ± 0.5	4.9	0.95
	Co–Zn	3.19	3.7 ± 0.1	2.8	
	Co–Zn	3.33	3.4 ± 0.1	2.8	
	Co–O	3.82	11.4 ± 0.9	4.9	

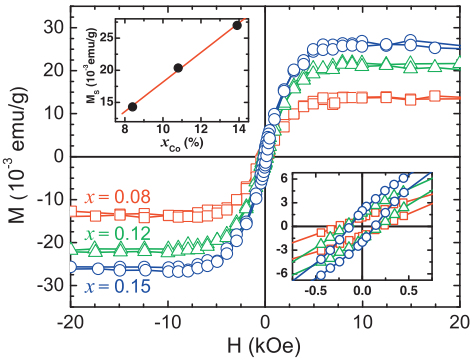

Fig. 4. Subtracting the paramagnetic contribution from magnetic moment measurements we clearly observe a ferromagnetic phase. The insets show the coercive field around 0.02 T (lower-right) and a linear saturation magnetization as a function of Co concentration (upper-left).

Table 3
Parameters of the magnetic characterization: effective Co concentration (x_E), number of Co atoms per gram (N_{Co}), saturation magnetization (M_S), paramagnetic susceptibility (χ_P), and estimated magnetic moment per Co atom (μ).

Sample (x)	x_E	N_{Co}/g ($\times10^{20}$)	M_S (emu/g)	χ_P ($\times10^{-6}$ emu/gOe)	μ (μ_B)
0.08	0.0843	6.2454	0.0143	7.25	4.10
0.12	0.1083	8.0261	0.02036	10.07	4.26
0.15	0.1386	10.2759	0.02698	12.20	4.14

(uncoupled Co spins), and k_B is the Boltzmann constant. On the other hand, the saturation magnetization of the ferromagnetic component is $M_S = \mu N_{FM}$, where N_{FM} is the number of Co atoms in the ferromagnetic phase (coupled Co spins). The total number of Co atoms (N_{Co}) can be assumed to be equal to the sum of N_{FM} and N_P. So, after a simple algebra, the value of μ can be estimated by solving the quadratic equation:

$$\mu^2 - \frac{M_S}{N_{Co}}\mu - \frac{3k_BT\chi_P}{N_{Co}} = 0 \quad (2)$$

We obtained an average value of 4.16 μ_B/Co atom (Table 3). This moment is much larger than the value of 1.72 μ_B/Co for cobalt metal, or that for small Co clusters (2.1 μ_B/Co) [28,29], or that of any of the standard Co oxides wherein the orbital moment is quenched. Such high moments per cation are inexplicable in terms of possible known ferromagnetic phases [30]. So, it is also evidence that the observed RTFM behavior is not due ferromagnetic secondary phases.

To elucidated the nature of the observed RTFM, the free carrier density of the samples was determined via Hall-effect measurements performed at room temperature in the standard van der Pauw geometry. The set of hydrogenated $Zn_{1-x}Co_xO$ samples are *n*-type semiconductors with decreasing of carrier concentration from 1.56×10^{14} to 0.2×10^{10} cm^{-3} as Co concentration increases. Considering the highly resistivity nature of our samples, neither the carrier-mediated *p-d* Zener model mechanism [1] nor the model proposed by Walsh et al. [6] can be applied to the low level itinerant electrons. On the other hand, at insulating regime the static magnetic polaron theory of Coey et al. [7] is more feasible. In this model, a spatial overlapping between one localized carrier trapped by a defect and the Co atoms within its orbit leads to ferromagnetic exchange coupling between them, forming a BMP.

Even more, we observe a linear relation between M_S and the Co concentration, if carrier-mediated exchange were the origin of RTFM, there would be no correlation between the dopant concentration and the magnetization, because carriers are not local. This behavior also exclude the possibility to address the correspondent RTFM to d^0 model, as it only takes into account the point/extended defects on the systems. Otherwise, in the context of the BMP model, a long range magnetic order occurs when two conditions are satisfied, the dopant concentration (x) have to be lower than the dopant percolation threshold (x_P) and the percentage of defects (δ) have to be larger than the polaron percolation threshold (δ_P), for the ZnO system $\delta_P = 0.0015$ and $x_P = 0.18$ [7]. Satisfying both condition, for the same density of defects (δ), by changing the Co concentration (x) we can linearly tune the saturation magnetization [31]. For our set of samples these two condition are satisfied. The highest effective Co concentration is only 0.1386 (<0.18), and, as pointed before in the DRX and Rietveld analysis, the density of defects for the samples are almost equal, an average value of 1.7% (0.017) for the V_O (>0.0015). Taking into account the depth action profile of the hydrogenation process, this number would be even bigger inside the volume of the sample close to the surface, where the ferromagnetic phase would be set. Therefore, the observed linear relation between the saturation magnetization and Co concentration is truly consistent with the BMP model.

4. Conclusion

In summary, in the absence of Co-rich nanocrystals and segregated secondary magnetic phases, the observed magnetic order in our samples is consistent with defect-induced ferromagnetism related to the hydrogenation process, consistent to the BMP theory developed to TM-doped oxides. The linear increasing of saturation magnetic moment as a function of Co concentration for same annealing process for all samples leads to conclusion that both conditions are necessary to achieve RTFM: the substitution of Zn by the Co dopant in the wurtzite ZnO structure in conjunction with the introduction of structural defects to mediate magnetic interaction between the Co atoms.

Acknowledgements

Support from agencies FAPEMIG, CNPq and FAPESP are gratefully acknowledged. The authors also acknowledge LNLS for the XAS measurements and the Electron Microscopy Laboratory (LME) of the Brazilian Nanotechnology National Laboratory (LNNano) for the HRTEM microscopy facilities.

References

[1] T. Dietl, H. Hono, F. Matsukura, J. Cibert, D. Ferrand, Zener model description of ferromagnetism in zinc-blende magnetic semiconductors, Science 287 (2000) 1019.

[2] M. Venkatesan, C.B. Fitzgerald, J.G. Lunney, J.M.D. Coey, Anisotropic ferromagnetism in substituted zinc oxide, Phys. Rev. Lett. 93 (2004) 177206.

[3] S.A. Chambers, S. Thevuthasan, R.F.C. Farrow, R.F. Marks, J.U. Thiele, L. Folks, M.G. Samant, A.J. Kellock, N. Ruzycki, D.L. Ederer, U. Diebold, Epitaxial growth and properties of ferromagnetic co-doped TiO_2 anatase, Appl. Phys. Lett. 79 (2001) 3467.

[4] A. Punnoose, J. Hays, V. Gopal, V. Shutthanandan, Room-temperature ferromagnetism in chemically synthesized $Sn_{1-x}Co_xO_2$ powders, Appl. Phys. Lett. 85 (2004) 1559.

[5] K. Ueda, H. Tabata, T. Kawaib, Magnetic and electric properties of transition-metal-doped ZnO films, Appl. Phys. Lett. 79 (2001) 88.

[6] A. Walsh, J.L.F. Da Silva, S.-H. Wei, Theoretical description of carrier mediated magnetism in cobalt doped ZnO, Phys. Rev. Lett. 100 (2008) 256401.

[7] J.M.D. Coey, M. Venkatesan, C.B. Fitzgerald, Donor impurity band exchange in dilute ferromagnetic oxides, Nat. Mater. 4 (2005) 173.

[8] M. Venkatesan, C.B. Fitzgerald, J.M.D. Coey, Thin films: unexpected magnetism in a dielectric oxide, Nature 430 (2004) 630.

[9] J. Alaria, J.M.D. Coey, Kwanruthai Wongsaprom, M. Venkatesan, Charged-transfer ferromagnetism in oxide nanoparticles, J. Phys. D: Appl. Phys. 41 (2008) 34012.

[10] H.B. de Carvalho, M.P.F. de Godoy, R.W.D. Paes, M. Mir, A. Ortiz de Zevallos, F. Iikawa, M.J.S.P. Brasil, V.A. Chitta, W.B. Ferraz, M.A. Boselli, A.C.S. Sabioni, Absence of ferromagnetic order in high quality bulk Co-doped ZnO samples, J. Appl. Phys. 108 (2010) 033914.

[11] Shuxia Guo, Zuliang Du, Influence of defects on magnetism of Co-doped ZnO, J. Magn. Magn. Mater. 324 (2012) 782.

[12] Y.H. Huang, Y.F. Liao, M.Z. Lin, C.H. Lee, J.F. Lee, S.F. Chen, L.Y. Lai, H.S. Hsu, J.C.A. Huang, C.P. Liu, Evidence of oxygen vacancy enhanced room-temperature ferromagnetism in Co-doped ZnO, Appl. Phys. Lett. 88 (2006) 242507.

[13] X.F. Qin, H.S. Wu, X.H. Xu, X.X. Li, Z.L. Wang, G.A. Gehring, Enhancement of magnetic moment of Co-doped ZnO films by postannealing in vacuum, J. Appl. Phys. 103 (2008) 023911.

[14] A. Samariya, R.K. Singhal, S. Kumar, Y.T. Xing, M. Alzamora, S.N. Dolia, U.P. Deshpande, T. Shripathi, E.B. Saitovitch, Defect-induced reversible ferromagnetism in Fe-doped ZnO semiconductor: an electronic structure and magnetization study, Mater. Chem. Phys. 123 (2010) 678.

[15] A.F. Kohan, G. Ceder, D. Morgan, C.G. Van de Walle, First-principles study of native point defects in ZnO, Phys. Rev. B 61 (2000) 15019.

[16] A. Singhal, Study of hydrogenation versus de-loading of Co and Mn doped ZnO semiconductor, J. Alloys Comp. 507 (2010) 312.

[17] A. Manivannan, P. Dutta, G. Glaspell, M.S. Seehra, Nature of magnetism in Co- and Mn-doped ZnO prepared by sol–gel technique, J. Appl. Phys. 99 (2006) 08M110.

[18] R.K. Singhal, A. Samariya, Y.T. Xing, S. Kumar, S.N. Dolia, U.P. Deshpande, T. Shripathi, E.B. Saitovitch, Electronic and magnetic properties of Co-doped ZnO diluted magnetic semiconductor, J. Alloys Comp. 496 (2010) 324.

[19] A.C. Larson, R.B. Von Dreele, General Structure Analysis System (GSAS), Los Alamos National Laboratory Report LAUR, vol. 86, 2000.

[20] B.H. Toby, EXPGUI, a graphical user interface for GSAS, J. Appl. Cryst. 34 (2001) 210.

[21] E.H. Kisi, M.M. Elcombe, Upsilon-parameters for the wurtzite structure of ZnS And ZnO using powder neutron-diffraction, Acta Crystallogr. Sect. C: Cryst. Struct. Commun. 45 (1989) 1867.

[22] R.D. Shannon, Revised effective ionic-radii and systematic studies of interatomic distances in halides and chalcogenides, Acta Crystallogr. Sect. A 32 (1976) 751.

[23] J. Pellicer-Porres, A. Segura, J.F. Sanchez-Royo, J.A. Sans, J.P. Itié, A.M. Flank, P. Lagarde, A. Polian, Tetrahedral versus octahedral Mn site coordination in wurtzite and rocksalt $Zn_{1-x}Mn_xO$ investigated by means of XAS experiments under high pressure, Superlatt. Microstruct. 42 (2007) 251.

[24] S.S. Hasnain. X-Ray absorption fine structure, in: Proc. Sixth International Conference on X-Ray Absorption Fine Structures (EXAFS and XANES), first ed., Ellis Horwood, Market Cross House, Cooper Street, Chichester, West Sussex, P.O. 19 1EB, 1991.

[25] A. Michalowicz, J. Moscovici, D. Muller-Bouvet, K. Provost, MAX: Multiplatform Applications for XAFS, J. Phys. Conf. Ser. 190 (2009) 012034.

[26] A.L. Ankudinov, B. Ravel, S.D. Conradson, J.J. Rehr, Real-space multiple-scattering calculation and interpretation of X-ray-absorption near-edge structure, Phys. Rev. B 58 (1998) 7565.

[27] S. Duhalde, M.F. Vignolo, F. Golmar, C. Chiliotte, C.E.R. Torres, L.A. Errico, A.F. Cabrera, M. Renteria, F.H. Sanchez, M. Weissmann, Appearance of room-temperature ferromagnetism in Cu-doped $TiO_{2-\delta}$, Phys. Rev. B 72 (2005) 161313.

[28] J.P. Bucher, D.C. Douglass, L.-A. Bloomfield, Magnetic properties of free cobalt clusters, Phys. Rev. Lett. 66 (1991) 3052.

[29] H.-J. Fan, C.-W. Liu, M.-S. Liao, Geometry, electronic structure and magnetism of small Con (n = 2–8) clusters, Chem. Phys. Lett. 273 (1997) 353.

[30] J.B. Goodenough, Magnetism and the Chemical Bond, Interscience, New York, 1963.

[31] C. Song, K.W. Geng, F. Zeng, X.B. Wang, Y.X. Shen, F. Pan, Y.N. Xie, T. Liu, H.T. Zhou, Z. Fan, Giant magnetic moment in an anomalous ferromagnetic insulator: Co-doped ZnO, Phys. Rev. B 73 (2006) 024405.